

1 Spin-polarized Density of states Calculation for Radicals

Inspired by the spin-polarized DOS calculations in the solid-state community, α and β eigenvalues were convoluted by a Gaussian function and small broadening. These calculations yield an intuitive picture of the spin-polarization over the HOMO level energy neighborhood and provide a qualitative explanation for the possible HOMO-SOMO inversion in this compound.

To analyze our studying cases' electron distribution, we calculated the total density of α and β states for all the proposed structures. $\Delta DOS(E)$ is defined as the difference between $DOS^\alpha(E)$ and $DOS^\beta(E)$ to inspect spin polarization of the system as function of energy. The results of $DOS(E)$ are shown in Figs. S1-S3 for cysteine, DOPA, and cystine radicals, respectively.

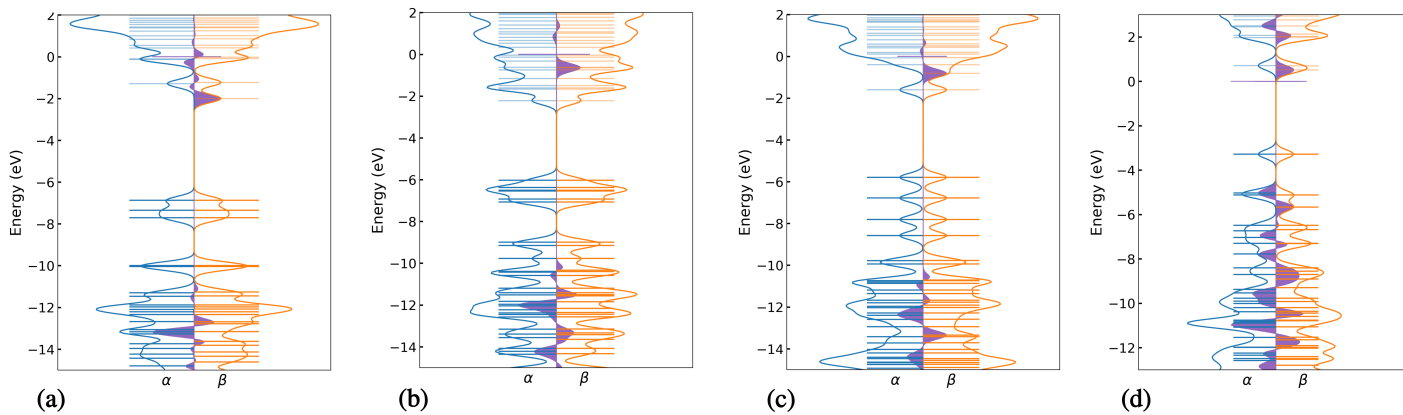


Figure S1 Eigenvalues and DOS plots of α (blue) and β (orange) molecular orbitals for (a) QCA, (b) RCE, (c) YCM and (d) YCM-RYC sequences.

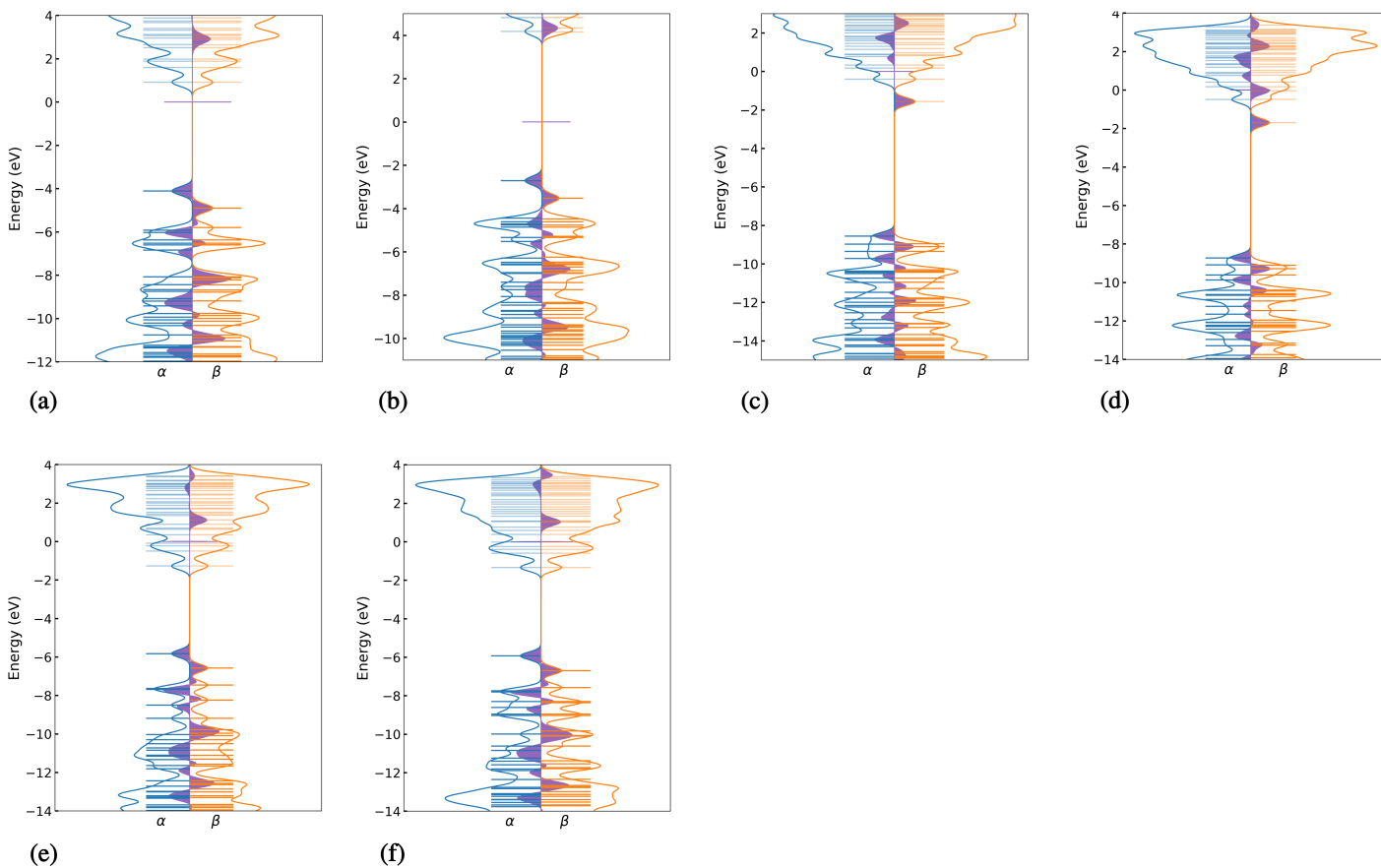


Figure S2 Eigenvalues and DOS plots of α (blue) and β (orange) molecular orbitals for (a) EYK, (b) EYQ, (c) RYC, (d) RYC-YCM, (e) TYR1, and (f) TYR2 sequences.

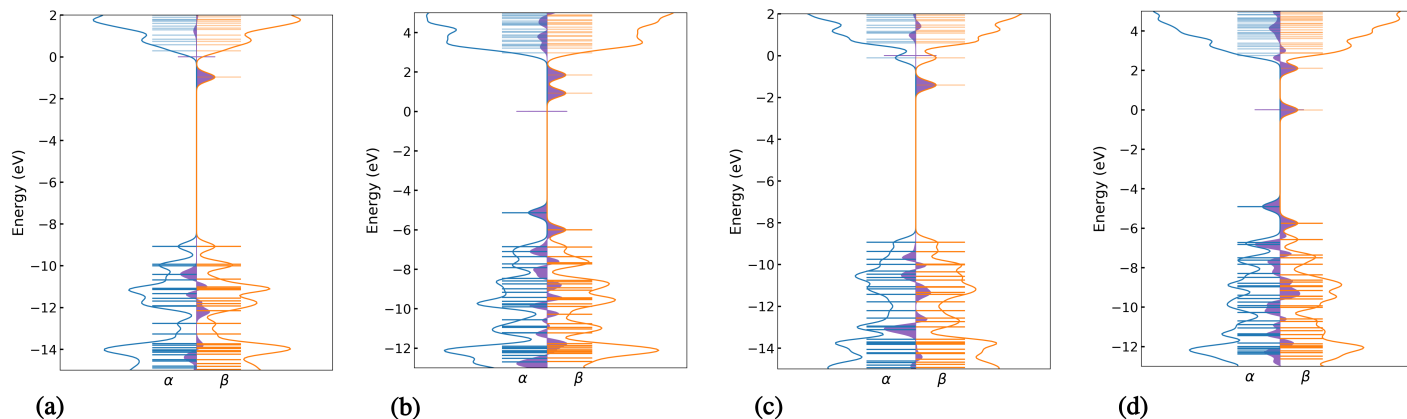


Figure S3 Eigenvalues and DOS plots of α (blue) and β (orange) molecular orbitals for (a) RSO, (b) RYC-RSO, (c) RSS and (d) RYC-RSS sequences.

As depicted in the above pictures, the obtained function is highly fluctuating near the HOMO level. The **cumulative sum** of $\Delta DOS(E)$ is defined to gain more in-depth insight into the system polarization. CSDOS(E) shows us the energy state after which there is no considerable fluctuation of $\Delta DOS(E)$. The most important analysis of this quantity is finding the energy region responsible for spin polarization; hence we can detect the probable SOMO-HOMO inversions.

CSDOS(E) curve has a smooth behavior near the HOMO with a value equal to the number of unpaired electrons, and fluctuations begin below the HOMO energy. Paying attention to the fluctuating region at the more profound energies, we can see that $DOS^\alpha(E)$ and $DOS^\beta(E)$ compensate each other until the specified region, where we can see a net difference showing as a plateau, and it can be interpreted as an unpaired electron indicator. The results of $\Delta DOS(E)$ are shown in Figs. S4-S6 for cysteine, DOPA, and cystine radicals, respectively.

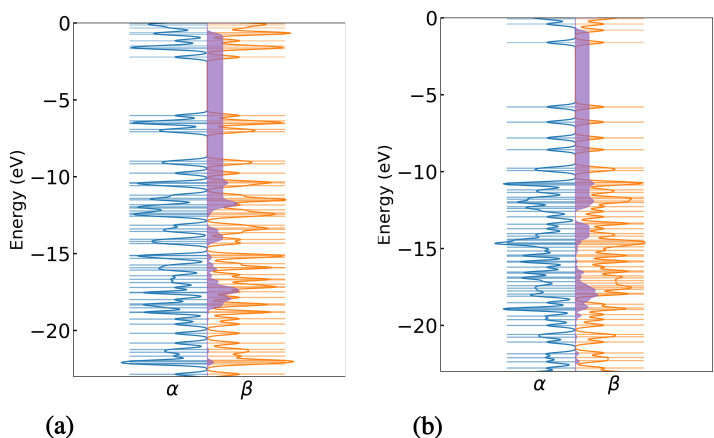


Figure S4 Eigenvalues and DOS plots of α (blue) and β (orange) molecular orbitals for (a) RCE, and (b) YCM sequences. Filled magenta curve shows the cumulative sum of $\Delta DOS(E)$. In the magenta curve it is shown that in the flat regions spin polarization does not change anymore. This region is the energy threshold in which the $\Delta DOS(E)$ does not fluctuate. Hence, the eigen-states below this energy level are responsible for the imbalance of α and β DOS, and spin polarization.

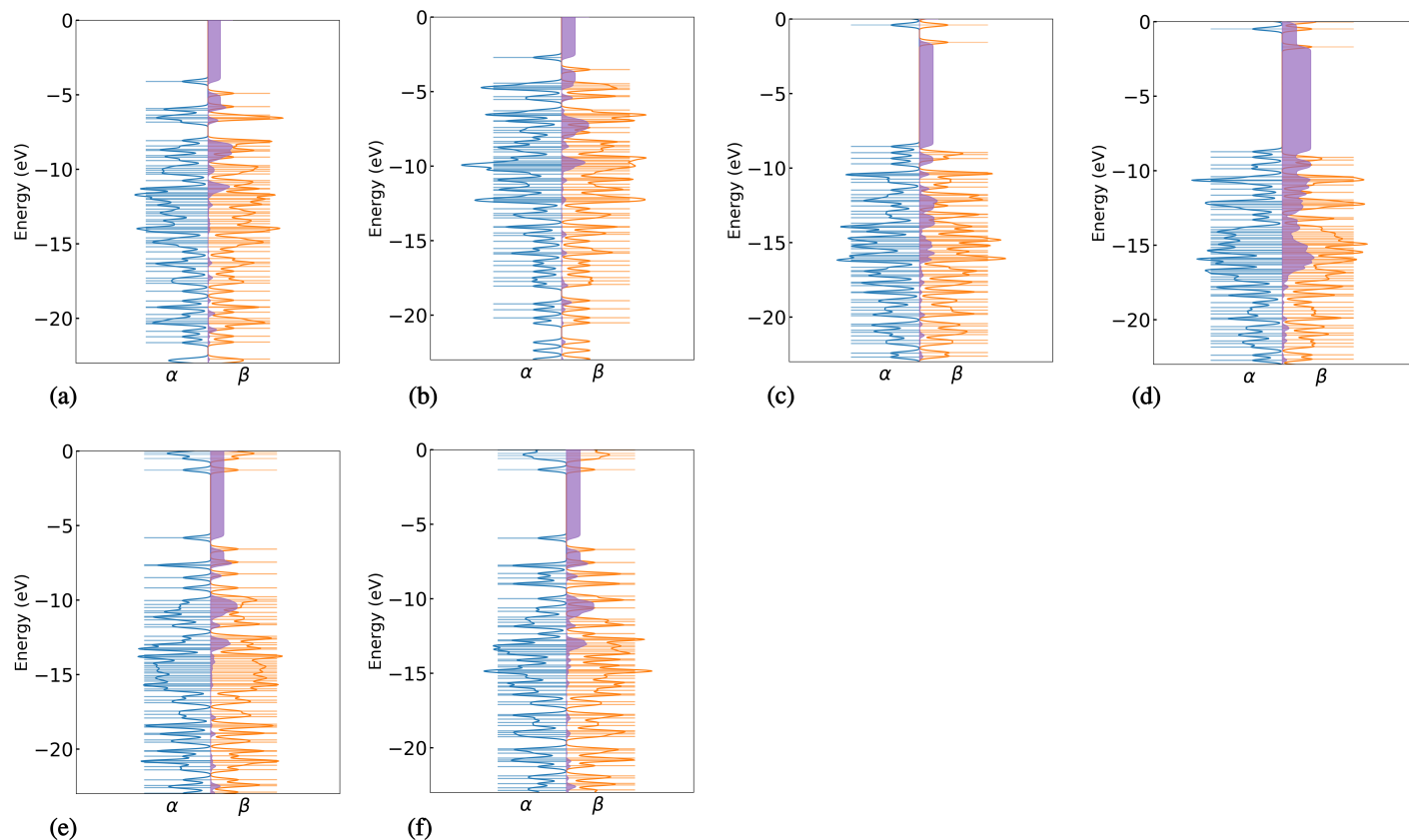


Figure S5 Eigenvalues and DOS plots of α (blue) and β (orange) molecular orbitals for (a) EYK, (b) EYQ, (c) RYC, (d) RYC-YCM, (e) TYR1, and (f) TYR2 sequences. Filled magenta curve shows the cumulative sum of $\Delta DOS(E)$. In the magenta curve it is shown that in the flat regions spin polarization does not change anymore. This region is the energy threshold in which the $\Delta DOS(E)$ does not fluctuate. Hence, the eigen-states below this energy level are responsible for the imbalance of α and β DOS, and spin polarization.

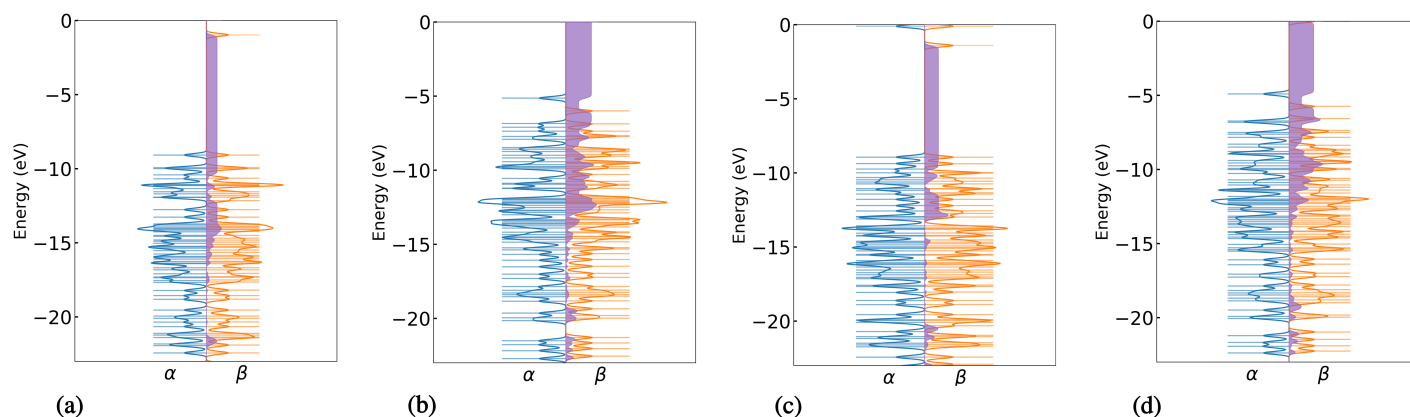


Figure S6 Eigenvalues and DOS plots of α (blue) and β (orange) molecular orbitals for (a) RSO, (b) RYC-RSO (c) RSS, and (d) RYC-RSS sequences. Filled magenta curve shows the cumulative sum of $\Delta DOS(E)$. In the magenta curve it is shown that in the flat regions spin polarization does not change anymore. This region is the energy threshold in which the $\Delta DOS(E)$ does not fluctuate. Hence, the eigen-states below this energy level are responsible for the imbalance of α and β DOS, and spin polarization.

We expect to see two plateaux for the CSDOS(E) curve of diradicals, representing two SOMO orbitals as two unpaired electrons exist. Checking the sharp peaks' locations, we can notice that we can not attribute a specific energy level to SOMO, but a set of orbitals with various contributions is involved. The energy windows where the SOMO is befallen is depicted in Table S1.

Table S1 qualitative SOMO depth of different radicals

Sequence	E-range of first radical (eV)	E-range of second radical
Thiyl Peroxyl		
QCA	[-20,-12]	
RCE	[-13,-10]	
YCM	[-20,-14]	
YCM-RYC	[-12,-8]	[-8,-5]
Tyrosyl Phenoxy		
EYK	[-7,-5]	
EYQ	[-6,-3]	
RYC	[-11,-8]	
RYC-YCM	[-17,-12]	[-12,-8]
TYR1	[-8,-5]	
TYR2	[-8,-5]	
Other Thiol Radicals		
RSO	[-17,-10]	
RYC-RSO	[-15,-8]	[-8,-5]
RSS	[-12,-10]	
RYC-RSS	[-15,-7]	[-7,-5]

2 Spin Contamination

Table S2 Impact of theory on spin contamination for QCA and YCM-RYC

	QCA-PBE	QCA-BLYP	QCA-LCBLYP	QCA-HF	YCMrr-PBE	YCMrr-BLYP	YCMrr-LCBLYP	YCMrr-HF
$\langle S^2 \rangle$ before annihilation	0.7929	0.8002	0.7540	0.7640	2.0122	2.1130	2.0963	2.8315
$\langle S^2 \rangle$ after annihilation	0.7502	0.7502	0.7500	0.7501	2.0001	2.0013	2.0029	2.3802

One of the common errors in spin calculation is spin contamination. Spin contamination results in wave functions with some spin states other than the desired mixed in. High spin contamination can affect the geometry and population analysis and significantly affect the spin density. As a check for the presence of spin contamination, most ab-initio programs will print out the expectation value of the total spin, $\langle S^2 \rangle$. If there is no spin contamination, this should equal $S(S+1)$ where S equals $1/2$ times the number of unpaired electrons. According to organic molecule calculations, if the value of $\langle S^2 \rangle$ differs from $S(S+1)$ by less than 10%, the spin contamination is negligible. Spin contamination is often seen in unrestricted Hartree-Fock (UHF) calculations and unrestricted Moller-Plesset (UMP2, UMP3, UMP4) calculations. It is less common to find any significant spin contamination in DFT calculations, even when unrestricted Kohn-Sham orbitals are being used. The impact of different levels of theory on spin contamination was examined. Two sequences were chosen for this purpose, one is the QCA with a radical, and the other is YCM-RYC with two radicals. The results are in the Table. S2. The chosen theory has not affected the results.

3 Signal broadening due to dynamics

To have a better estimation for the broadening factor, we applied an MD simulation on α -keratin protein. Then, we separated 60 random snapshots for each QCA, RCE, YCM, and YCM-RYC sequences and calculated a range of g -tensors for those snapshots. We plotted the magnetic fields using a Gaussian distribution to broaden the spectrum in the next step. The distributions of g -tensor components for cysteine radicals are depicted in Fig. S7- S9.

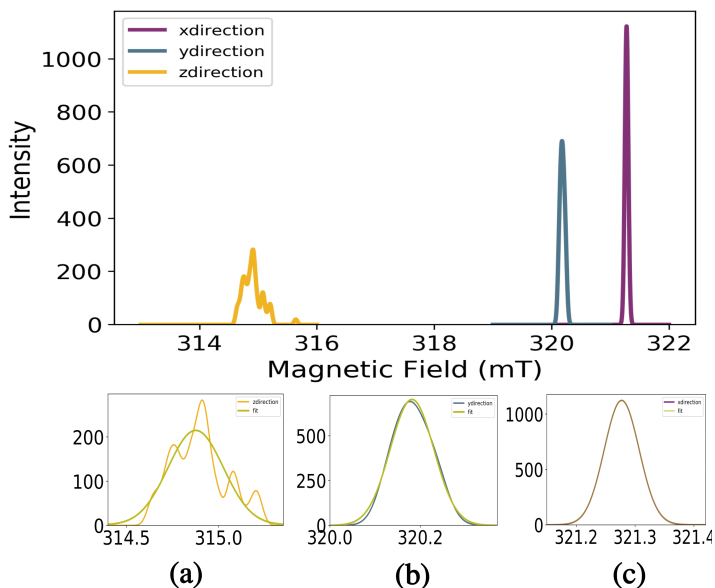


Figure S7 Fitted Gaussian functions for three dimensions of RCE's EPR spectra in (a) z direction, (b) y direction, and (c) x direction. Sixty snapshots were chosen randomly from MD simulation of RCE sequence to calculate the g -value for each of the sixty inputs. The magnetic field corresponding to the g -values were calculated and plotted. The broadening (σ) of these distributions corresponds to broadening due to dynamics.

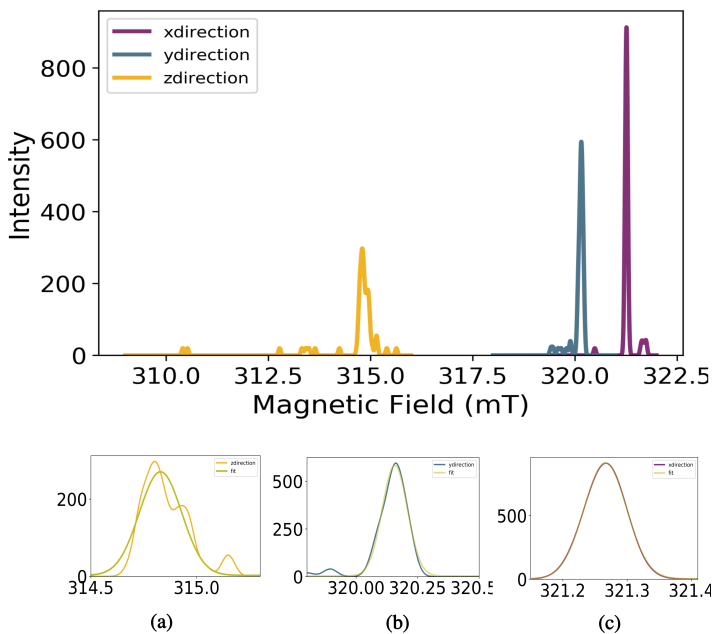


Figure S8 Fitted Gaussian functions for three dimensions of YCM's EPR spectra in (a) z direction, (b) y direction, and (c) x direction. Sixty snapshots were chosen randomly from MD simulation of YCM sequence to calculate the g -value for each of the sixty inputs. The magnetic field corresponding to the g -values were calculated and plotted. The broadening (σ) of these distributions corresponds to broadening due to dynamics.

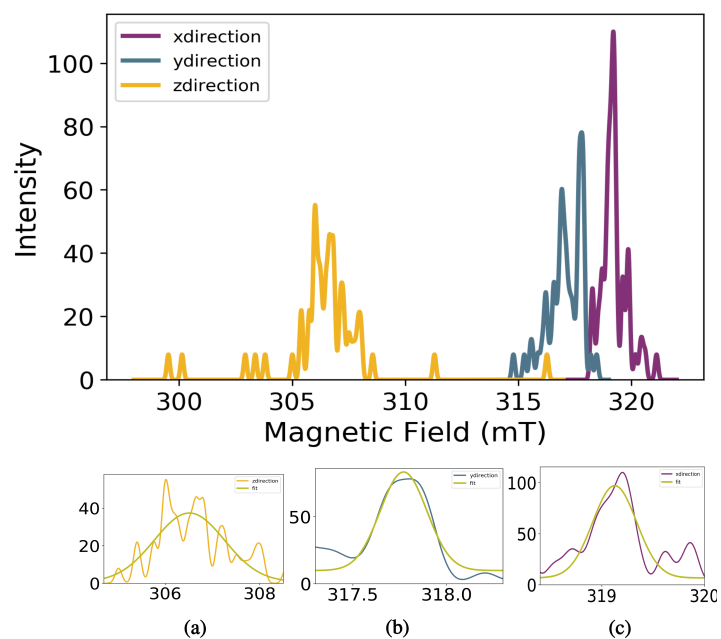


Figure S9 Fitted Gaussian functions for three dimensions of YCM-RYC's EPR spectra in (a) z direction, (b) y direction, and (c) x direction. Sixty snapshots were chosen randomly from MD simulation of YCM-RYC sequence to calculate the g-value for each of the sixty inputs. The magnetic field corresponding to the g-values were calculated and plotted. The broadening (σ) of these distributions corresponds to broadening due to dynamics.

4 Reported g-tensors in literature

Possible radical centers formed in irradiated keratin proteins are depicted in Table S3. It is worth mentioning that most of the sulfur radicals depicted here are not stable enough to be considered as the responsible radical center in nail dosimetry. They will be eliminated in water or via temperature treatments, and they are mostly considered as MIS.

Table S3 Literature review of g-tensors in sulfur and tyrosyl radicals

Radical	method	g_{xx}	g_{yy}	g_{zz}	ref
RS	exp.	2.000	2.024	2.060	10.1111/j.1751-1097.1972.tb06258.x
RS	exp.	1.997	2.011	2.024	10.1007/978-3-7091-1007-2
RSS	exp.	1.996	2.026	2.056	10.1097/HP.0b013e3181b0c045
RSS	exp.	1.997	2.011	2.056	10.1007/978-3-7091-1007-2
RSS	exp.	1.998	2.023	2.055	10.1007/s00411-014-0512-2
RSS	exp.	2.0019	2.026	2.056	10.1080/09553008814551121
RSS	exp.	2.002	2.027	2.057	10.1039/b302601a
RSS	exp.	2.000	2.026	2.053	10.1016/S0009-2614(00)00961-1
RSS	cal.	2.002	2.028	2.063	10.1016/S0009-2614(00)00961-1
RSS	cal.	2.002	2.0313	2.075	This work
RSSR	exp.	2.000	2.025	2.061	10.1038/328833a0
RSSR	exp.	2.000	2.025	2.061	10.1093/oxfordjournals.rpd.a082591
RSO	exp.	-	-	2.020	10.1039/b302601a
RSO	exp.	2.0027	2.0094	2.024	10.1080/09553008814551121
RSO	exp.	2.003	2.008	2.025	10.1007/s00411-014-0512-2
RSO	cal.	2.0024	2.015	2.028	This work
RSO2	exp.	2.0021	2.0079	2.0104	10.1093/rpd/ncw216
RSO2	exp.	2.008	-	-	10.1039/b302601a
RSO2	exp.	2.0034	2.0053	2.0070	10.1063/1.1676486
RSO2	exp.	2.006	2.034	2.034	10.1039/b302601a
RSO2	exp.	2.0017	2.0084	2.0328	10.1093/rpd/ncw216
RSO2	cal.	2.00178	2.00908	2.04183	This work
Tyrosyl	exp.	2.002	2.0042	2.0087	10.1021/ja00148a013
Tyrosyl	cal.	2.0025	2.0050	2.0087	10.1021/jp0006633
Tyrosyl	cal.	2.002	2.0054	2.0085	10.1021/ja0162764
Tyrosyl phenoxyl	exp.	2.0024	2.0042	2.0066	10.1021/jp710 220u
Tyrosyl phenoxyl	cal.	2.0022	2.0053	2.0063	10.1093/rpd/ncw216
Tyrosyl phenoxyl	cal.	2.00217	2.00716	2.00763	This work